Electron Temperature of Optically Ionized Gases Produced by High Intensity 268 nm Laser Radiation

A. A. Offenberger,[1,*] W. Blyth,[1] A. E. Dangor,[2] A. Djaoui,[3] M. H. Key,[3,†] Z. Najmudin,[2] and J. S. Wark[1]

[1]*Department of Physics, Clarendon Laboratory, University of Oxford, Oxford OX1 3PU, United Kingdom*
[2]*Department of Physics, Blackett Laboratory, Imperial College of Science, Technology and Medicine, London SW7 2BZ, United Kingdom*
[3]*Rutherford Appleton Laboratory, Chilton, Didcot, Oxon OX11 0QX, United Kingdom*
(Received 9 August 1993)

Thomson scattering measurements have been used to determine the electron energy distribution in UV optically ionized He and Ne at pressures up to $\frac{1}{2}$ bar irradiated at 3×10^{17} W/cm^2 in 12 ps. The electrons evolve from a multiphoton ionization spectrum to a thermal distribution with increasing pressure. The low frequency part of the scattered spectrum clearly shows the "zero-damped" ion acoustic mode for high values of ZT_e/T_i. Experimental and modeling results indicate that nonlinear inverse bremsstrahlung heating and radial conduction cooling dominate the electron energy balance.

PACS numbers: 52.40.Nk, 52.25.Qt, 52.50.Jm

Optically ionized gases are of considerable interest for their potential to produce "cold" multiply ionized plasmas that may provide suitable media for extreme ultraviolet (XUV) recombination lasers [1–3]. A key requirement for the feasibility of such schemes is that the electron temperature be much lower than the ionization potential in order to maximize the population inversion in the recombination cascade. At the high laser intensities required for optical ionization schemes (e.g., Li-like Ne or H-like B), however, some electron heating will be unavoidable. It is therefore important to determine experimentally the role and consequences of heating mechanisms such as above threshold ionization (ATI), nonlinear inverse bremsstrahlung (IB) absorption, and stimulated Raman scattering (SRS) in optically ionized gases [1,3–6]. For the required laser intensities (10^{17}–10^{18} W/cm^2), calculations show that short wavelength lasers and ultrashort pulses will be needed to minimize heating.

We have made a study of these phenomena using 268 nm laser radiation at a focused intensity of 3×10^{17} W/cm^2 to meet the theoretical requirements identified above but in a pulse of 12 ps duration which is longer than optimal but which enhances the role of IB and SRS heating relative to ATI and introduces significant cooling during the pulse through radial thermal conduction. Here we report electron temperature measurements in helium and neon with the particular objective of determining the relative roles of the mechanisms identified above.

Since it is important to determine the temperature T_e during the laser pulse and within the laser beam, we have used 90° Thomson scattering of the incident beam to measure directly the electron distribution function. This technique is better suited to temperature measurements than using XUV emission [7] which, as a consequence of time and volume integration, tends to underestimate T_e. Importantly, for the conditions of the present experiment, optical ionization occurs in a time short compared to the 12 ps (FWHM) laser pulse duration; consequently, Thomson scattering of the incident beam enables a measurement of the electron distribution during the bulk of the heating period following ionization. Calculations we have made [8] show that T_e increases roughly linearly with time during the 12 ps pulse; consequently, time integrated Thomson scattering measurements will give results characteristic of conditions at the midpoint of the pulse. Simultaneous measurements at 180° showed enhanced scattering due to the onset of stimulated Brillouin and stimulated Raman scattering (SBS and SRS) and provided independent temperature and density information, details of which will be reported in a separate publication.

The experiments used the SPRITE KrF laser facility operating as a KrF laser pumped Raman laser [9], generating 0.25 TW power at 268 nm wavelength with less than 10^{-10} prepulse. The 8 cm laser beam with typical energy of 3 J in a pulse of 12 ps (FWHM) duration was focused by a 33 cm focal length parabolic mirror into gas at the center of an 80 cm diameter vacuum chamber. The vertically polarized laser beam contained $\frac{1}{2}$ of the energy in a 3× diffraction limited focal spot (diameter 6.5 μm) and the remainder in a 9× diffraction limited focal spot (diameter 20 μm), giving peak intensity in the central region up to 7×10^{17} W/cm^2. Data recorded at static gas pressures up to 400 Torr in He and Ne will be reported here. Other data (and analysis) for H_2 and Kr with static and gas jet targets up to 10 bars pressure together with measurements of SBS and SRS will be reported elsewhere.

Thomson scattered light was collected at 90° to both the incident beam and polarization directions; thus the wave number of the density fluctuations probed is given by $k=2k_0\sin(\theta/2)=\sqrt{2}\omega_0/c$. The scattered light from the focused high intensity beam was optically imaged using chromatically corrected lenses with magnifications of either 3× (two lenses) or 10× (single lens) onto the en-

0031-9007/93/71(24)/3983(4)$06.00

trance slit of a Czerny Turner monochromator (0.3 m, $f/4$, 1200 g/mm grating) coupled to a streak camera–intensified charge coupled device system. The 1 cm spectrometer input slit was oriented parallel to the laser beam axis and the streak direction was perpendicular to the dispersion direction. The streak camera was used to discriminate the relatively weak prompt Thomson scattered light from the delayed stray light. For the 50–100 ps/mm streak speeds used, the axially resolved spectrum was recorded with negligible blur due to streaking. Since the 100 μm input slit was wider than the image of the focus over the central ± 500 μm length of the focused beam, the scattered light gave a radially integrated (≈ 40 μm resolution) but axially resolved measurement of plasma conditions.

Typical Thomson scattered spectral profiles at the focal point for three different static pressures of He and Ne are shown in Figs. 1 and 2, respectively. For low pressure He and Ne (≈ 1 Torr), the spectra are characteristic of a multiphoton ionized (ATI heated) electron energy distribution [10]. While it is not rigorously possible to define a temperature at low pressure (since the electron collisional relaxation time is of the order of the laser pulse duration), Gaussian distributions with characteristic "temperatures" of $T_e = 6.5$ and 6.8 eV for He and Ne, respectively, have been convolved with the instrument width of 0.7 nm and overlaid on the data to indicate an upper bound on the electron energy.

The high pressure (≥ 10 Torr) experimental spectra of Figs. 1 and 2 have been fitted (dashed lines) by theoretical Thomson scattering form factors (discussed below). Several important characteristics can be observed in these scattered spectra. In the first place, the high frequency parts of the spectra are found to be symmetrical and therefore correspond to scattering from thermal electrons; in contrast, enhanced redshift signals would be observed for SRS. Second, the agreement between calculated and experimental spectra for frequency shift $\omega \approx \pm \omega_{pe}$ shows that ponderomotive effects are not important since nonthermal electron plasma oscillations would otherwise be observed. Third, these results show that the spectra evolve from ones characteristic of ATI at low pressure to thermal electron distributions at moderate pressure. This behavior is to be expected for higher density where the electrons have sufficient time to thermalize.

Finally and significantly, in addition to the normal high frequency "electron" feature, Figs. 1 and 2 show that a distinct low frequency "ion" feature emerges with increasing pressure. The theoretical "ion" feature has a width less than the experimental 0.7 nm spectral resolution. From the dynamic form factor for scattering from thermal density fluctuations [11],

$$S(k,\omega) = S_e(k,\omega) + S_i(k,\omega) = \frac{|1+\chi_i|^2 f_e(\omega/k)}{|1+\chi_e+\chi_i|^2} + \frac{Z|\chi_e|^2 f_i(\omega/k)}{|1+\chi_e+\chi_i|^2},$$

where $f_{e,i}(\omega/k)$ are the one-dimensional Maxwell-Boltzmann distributions and $\chi_{e,i}$ are the electron (ion) susceptibilities, it can be shown that the fraction of scattered light arising from the normal ion feature S_i is negligible for $ZT_e/T_i \gg 1$. The electron feature S_e, however, displays an important resonance—the "zero-damped" ion acoustic mode—for large ZT_e/T_i, in addition to the normal electron thermal feature. From the real part of the dielectric function, it can be shown that the minimum temperature ratio required for this resonance is given by $1+\alpha^2-0.29\alpha^2 ZT_e/T_i = 0$, where $\alpha = 1/k\lambda_D$. In this situation, not normally accessible experimentally, the spectrum of scattered light admits the determination of T_e/T_i

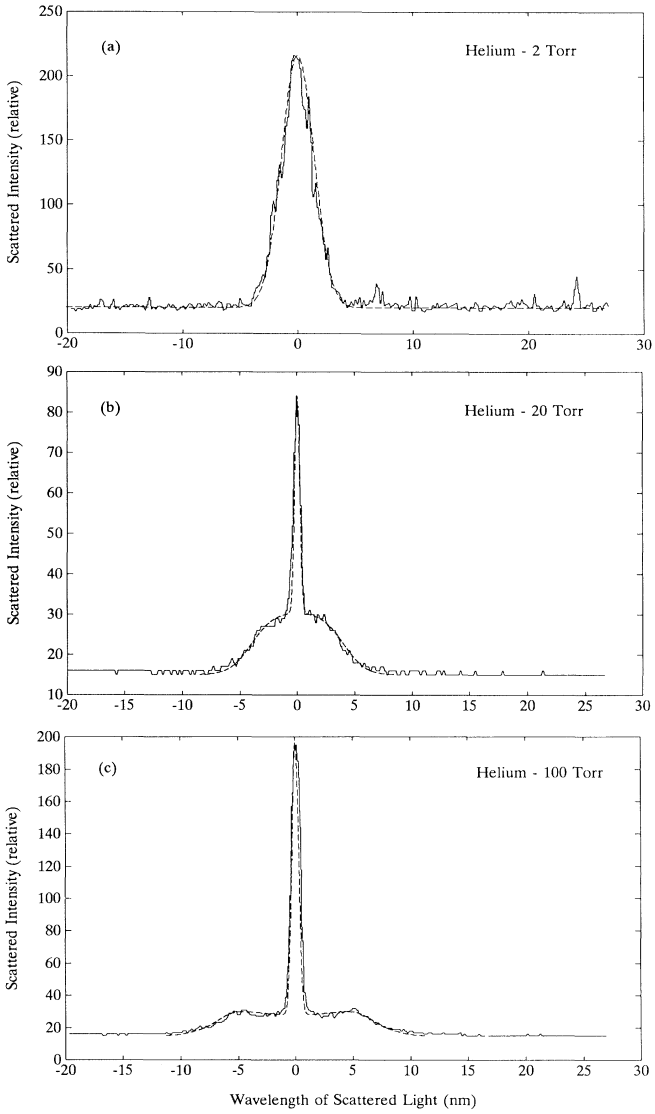

FIG. 1. Thomson scattered spectra for He at various pressures. A 6.5 eV Maxwell-Boltzmann distribution (dashed line) is overlaid on the 2 Torr data to give an upper bound on electron energy. The electron spectral fits $S(k,\omega)$ shown as dashed lines are calculated for $T_e = 20.6$ eV and $\alpha \approx 0.65$ (20 Torr); $T_e = 36$ eV and $\alpha \approx 1.1$ (100 Torr).

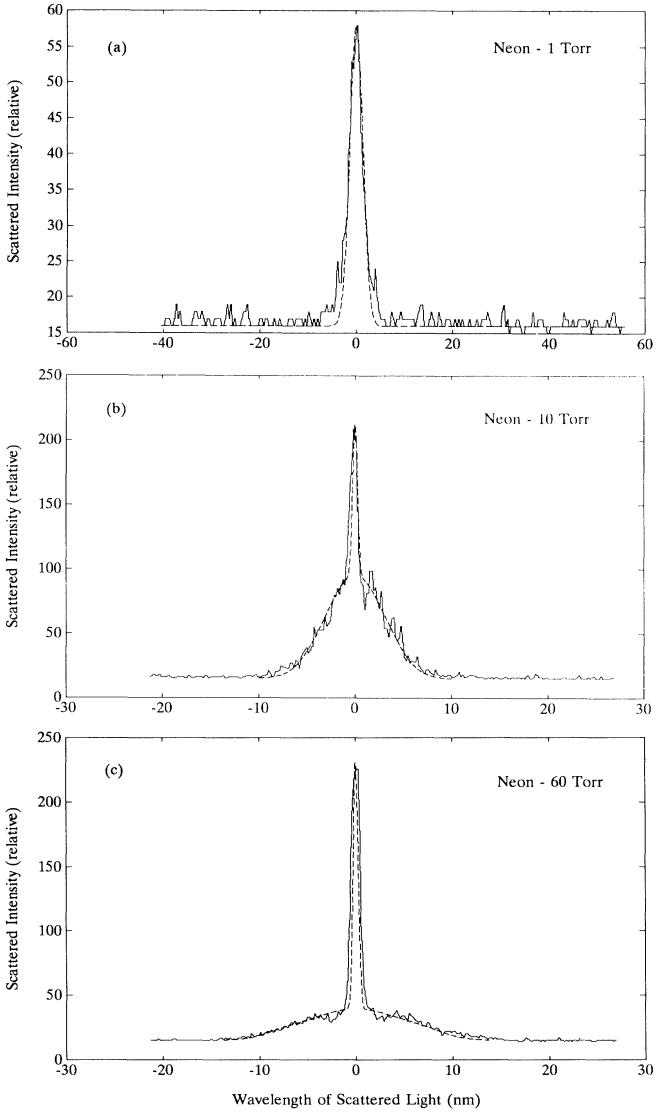

FIG. 2. Thomson scattered spectra for Ne at various pressures. A 6.8 eV Maxwell-Boltzmann distribution (dashed line) is overlaid on the 1 Torr data to give an upper bound on electron energy. The electron spectral fits $S(k,\omega)$ shown as dashed lines are calculated for $T_e = 28.5$ eV and a mixture of $\alpha = 0$ and $\alpha = 0.7$ (10 Torr); $T_e = 64.2$ eV and a mixture of $\alpha = 0$ and $\alpha = 1$ (60 Torr). These fits are only approximate since the temporal and spatial distribution of ionization Z is unknown.

(within limits) from the ratio of scattering into low and high frequency components, as well as T_e from the width of the high frequency component. This evolution can be seen for He in Fig. 1 where the measured spectra have been fitted by theoretical Thomson scattering form factors (fitting Ne is more difficult because of volume and time averaging effects over variable Z of the ion states). The calculated curves are a convolution of the monochromator instrument function (0.7 nm FWHM) and theoretical $S(k,\omega)$. We conclude that the low frequency feature

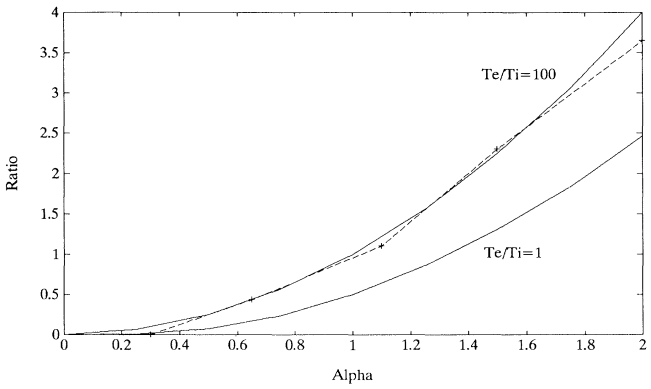

FIG. 3. Experimental ratio of scattering in the central "ion" feature to that in the "electron" feature as a function of He gas pressure (experimental points, dashed curve). The calculated ratios for limiting values of $T_e/T_i = 1$ and 100 [from the full $S(k,\omega)$ equation], are shown as solid lines. The estimated errors are $\pm 10\%$ in α and $\pm 15\%$ in ratio.

results from the zero-damped ion mode resonance in the electron term of the scattering form factor. The results are of particular interest because the very high values of ZT_e/T_i are responsible for the dominance of the zero-damped feature which, to our knowledge, has not been reported before.

The experimental ratio of integrated scattering in the central "ion peak" to that in the outer "electron" wings is plotted as a function of scattering parameter $\alpha = 1/k\lambda_D$ in Fig. 3. Also shown is the calculated ratio for T_e/T_i values of 1 and 100 (it can be shown that the ratio varies as α^2 and increases with T_e/T_i reaching a limiting value when T_e/T_i exceeds 10–100, depending on α). Thus our experimental data indicate $T_e/T_i > 10$ for $\alpha \approx 2$ and $T_e/T_i > 50$ for $\alpha \approx 0.5$. We conclude that high field optical ionization results in a large T_e/T_i ratio; however, the accuracy of our experimental determination of this ratio is limited, particularly at low pressure.

The electron temperatures deduced for He and Ne as a function of pressure are summarized in Fig. 4. For Ne, however, it is important to note that the experimentally derived temperatures are an upper bound determined by an approximate spectral fitting to the measured spectra. Since the experimental spectra are volume and time integrated averages over ionization state Z, the actual spatial and temporal variations for Ne preclude analysis comparable to that for He, which has a known ionization state $Z = 2$ during the Thomson scattering period. We have calculated spectra for varying Z and α (i.e., varying n_e, T_e with concomitant varying α) which indicate that mixed α spectral fitting may overestimate T_e by a factor of up to 2 for Ne.

The experiment was modeled using a one-dimensional hydrodynamic and time dependent ionization code (details to be published separately [8]). Above threshold ionization heating, nonlinear inverse bremsstrahlung absorption, and lateral electron thermal conduction losses

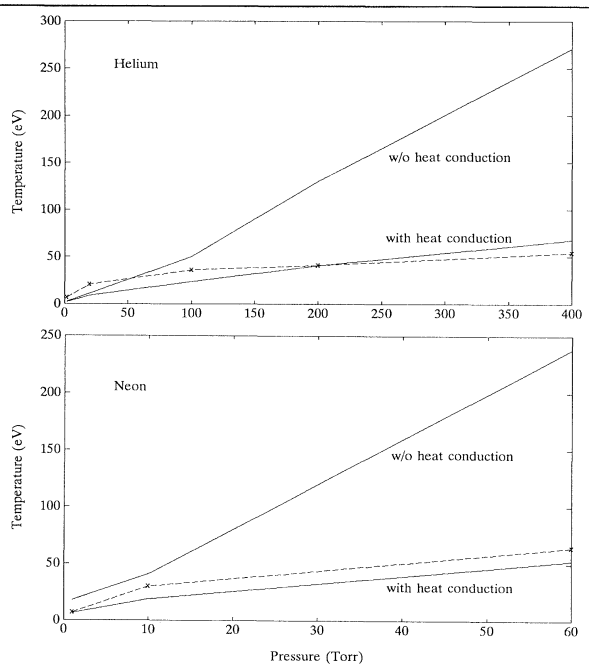

FIG. 4. Experimental T_e scaling with pressure for He and Ne (data points and dashed curves). The solid curves are calculated values using a code that includes above threshold ionization heating, nonlinear inverse bremsstrahlung heating, and radial electron thermal conduction cooling. The experimental T_e for Ne is likely an overestimate, for reasons discussed in the text.

are included in the model. Figure 4 shows the calculated temperature on axis at the peak of the laser pulse. Important points to note are the following: (1) In the absence of radial electron heat conduction losses, the calculated T_e would be much higher and increase linearly with pressure, at variance with the measured values and pressure variation for He; (2) the calculated ATI heating is found to be negligible compared to IB heating for our experimental parameters; (3) the experimental and calculated T_e values agree quite well for both He and Ne, indicating that classical electron thermal conduction losses are important for the laser intensity and pulse duration conditions of this experiment (discrepancies are likely due to experimental volume and time averaging effects, as discussed above).

Spatial measurements of the axially resolved Thomson scattered light were also made to determine the ionization profile in the focal region. The scattered intensity profile was observed to increase and decrease monotonically through the focus over a length of ≈ 1 mm for He and Ne; moreover, there is no axial modulation in scattering which would be a signature of self-focusing. For low pressure (≈ 1 Torr), the spectrum is broader at the focus than upstream or downstream whereas for moderate pressure (> 10 Torr), the spectral width is axially uniform over several hundred microns. For the conditions of this experiment ($\lambda = 268$ nm, $f/4$ focusing optics), refraction is not expected (or observed) to play an important role [12].

In conclusion, the Thomson scattering results are consistent with an electron energy distribution evolving from a collisionless ATI distribution at low density to a thermal electron distribution at moderate density. The central feature of the scattered spectrum shows the presence of the "zero-damped" ion acoustic mode. The wings of the spectrum (at low to moderate pressure) do not show any evidence of SRS or of ponderomotive effects creating significant levels of electron plasma waves. Comparison with modeling establishes that ATI heating is unimportant relative to nonlinear inverse bremsstrahlung heating and that radial heat conduction broadens the heated region and reduces the electron temperature.

These results show that it is possible to create columns of "cold" plasma ($T_e < 50$ eV) by optical ionization and radial cooling of gases. For 100–200 fs pulses that will ultimately be employed for any practical XUV recombination scheme, inverse bremsstrahlung heating and radial conduction effects would be reduced. The agreement with modeling in this work suggests that predictions of conditions needed for XUV laser action with sub-ps pulses are well founded. Experiments to test this will be completed soon.

It is a pleasure to acknowledge the support of staff at the Rutherford Appleton Laboratory and the Science and Engineering Research Council fellowship award for A.A.O.

*Visiting from Department of Electrical Engineering, University of Alberta, Edmonton, Alberta, Canada T6G 2G7.
†Also at University of Oxford, Oxford, United Kingdom.

[1] N. H. Burnett and P. B. Corkum, J. Opt. Soc. Am. B **6**, 1195 (1989).
[2] N. H. Burnett and G. D. Enright, IEEE J. Quantum Electron. **26**, 1797 (1990).
[3] D. C. Eder, P. Amendt, and S. C. Wilks, Phys. Rev. A **45**, 6761 (1992).
[4] S. C. Rae and K. Burnett, Phys. Fluids B **2**, 1015 (1990).
[5] B. M. Penetrante and J. N. Bardsley, Phys. Rev. A **43**, 3100 (1991).
[6] S. C. Wilks, W. L. Kruer, A. B. Langdon, P. Amendt, D. C. Eder, and C. J. Keane, Lawrence Livermore National Laboratory Report No. UCRL-JC-106277, February 1991 (unpublished).
[7] A. Sullivan, S. P. Gordon, H. Hamster, H. Nathel, and R. W. Falcone, in Technical Digest of the Meeting on Short Wavelength Lasers V: Physics With Intense Laser Pulses, San Diego, 1993 (Optical Society of America, Washington, DC, to be published).
[8] A. Djaoui *et al.* (to be published).
[9] M. J. Shaw, G. Bialolenker, G. J. Hirst, C. J. Hooker, M. H. Key, A. K. Kidd, J. M. D. Lister, K. E. Hill, G. H. C. New, and D. C. Wilson, Opt. Lett. (to be published).
[10] N. B. Delone and V. P. Krainov, J. Opt. Soc. Am. **8**, 1207 (1991).
[11] D. E. Evans and J. Katzenstein, Rep. Prog. Phys. **32**, 207 (1969); E. E. Salpeter, Phys. Rev. **120**, 1528 (1960).
[12] S. C. Rae, Opt. Commun. **97**, 25 (1993).